International Journal of Innovative Computing, Information and Control
Volume **9**, Number **11**, November **2013**

ICIC International ©2013 ISSN 1349-4198
pp. 4471–4484

COLOR IMAGE SEGMENTATION USING A MORPHOLOGICAL GRADIENT-BASED ACTIVE CONTOUR MODEL

Nguyen Tran Lan Anh, Soo-Hyung Kim, Hyung-Jeong Yang and Guee-Sang Lee*

Department of Electronics and Computer Engineering
Chonnam National University
77 Yongbong-ro, Buk-gu, Gwangju 500-757, Republic of Korea
*Corresponding author: gslee@jnu.ac.kr

Received September 2012; revised February 2013

Abstract. *Segmenting objects of dynamic shapes and various colors is still challenging to the computer vision of natural images, because of slow computation, inaccuracy, and loss of information. In this paper, we propose a novel segmentation algorithm based on active contour models, to overcome these weaknesses. First, we apply a morphological gradient-based edge detector to an image, to extract its edge map. Because this step is performed directly on color images, it helps us avoid losing color characteristics, compared with gray-scale conversion. Second, this edge map will be used as a clue to provide both good edge information and good region information for an active contour, without a re-initialization model. As a result, our proposed algorithm allows the contour to be initialized more flexibly, evolves the contour faster, and segments the boundary of objects more precisely in color images. Results attained on diverse natural images show its promising performance, compared with other models, for both accuracy and computational time.*

Keywords: Morphological gradient, Chan-Vese criterion, Level set, Object segmentation, Color images

1. **Introduction.** Due to the explosion of digital information, color images have become one of the most popular data types. From the current viewpoint, they not only portray simple scenes, but also contain a great deal of useful information described by captured objects. However, large-size digital images are an obstacle to the performance of most processing systems. Hence, the demand for good methods of segmenting these objects in many devices cannot be neglected, especially in small-screen equipment (e.g., mobile devices). Since most segmentation methods still expect human operators to first initialize a contour close to the object boundary, they are likely time consuming and ineffective.

Therefore, the subject of segmenting objects of interest in images has gained even more attention. From the primary benefit of producing simple informative input, object segmentation is a foundational tool in various advanced systems, such as object recognition [1], image retrieval [2], image editing [3] and scene reconstruction [4]. Due to its significant role, this crucial step has been of perennial interest to many researchers of image processing and computer vision [5-10].

Active contour model (ACM) [11] is one of the representative tools for object segmentation and it finds object boundaries by iterative optimization. It has been used extensively for shape detection, object segmentation, especially in medical images taken from different pieces of equipment (i.e., PET, MRI and CT). It solves complicated and ill-posed segmentation problems by combining *a priori* boundary shape information with the image itself, and an initial shape given by the user. Generally, the main weaknesses of existing ACM

based methods are their dependence on the identification of high confidence instructions, initialization close to the object boundary, and the number of segmented regions. Most of all, initial contours of the ACMs need to be less complicated and requires exact user interactions.

The active contour model was first introduced by Kass et al. [11] in 1987, and is called 'snake'. In snake, a contour is defined by closed curves or surfaces. For segmenting dynamic shapes of objects in gray-scale images, a contour is first initialized, and then evolved to the boundary of objects under the influence of constraint forces from the image, by minimizing a specific user-defined energy functional. Snake models have been applied to many applications, despite a few problems associated with their initialization, and poor convergence to boundary concavities. Subsequently, Osher and Sethian [12] developed a level set method (LSM) to give a new solution of ACMs. Its basic idea is to represent the active contour as level sets of higher dimensional functions, yielding seamless treatment of topological changes. Various external forces, such as the gradient, or gradient vector flow embedded in the speed function, can be found in [13-18]. There are two expected properties of segmentation methods implemented through the level set framework. The first property is its suitability for handling complex and changeable topology, such as splitting and merging a contour. The other is its ability to perform numerical computations on a Cartesian grid, without concerning the parameterization of points on a contour.

ACMs are roughly divided into two categories, based on edge information and region information. For edge-driven models, edge descriptors are usually computed by using various types of gradient information to attract the active contour toward the object boundaries, which have a strong edge response. Due to local minimization and image noise, this type of approach is sensitive, and dependent on the initial front. For region-driven models, one establishes a certain region descriptor to take global information into account, and guides the movement of the active contour. Its information can be collected as the mean of partitioned regions [17], the weighted mean of the constrained or scalable neighboring regions [19], statistical information of the partitioned regions [20]. In comparison with edge-based approaches, region-based active contours are robust against initial curve placement, and have no need for *a priori* noise removal.

Many studies have concentrated on the disadvantages of ACMs. First, to overcome the problem of cognitive edges in gray-scale images, Chan and Vese [17] proposed a model named active contour without edges. Its solution was simple but effective among region-driven models in the level set framework. Their idea, named the Chan-Vese minimal variance criterion, has become a useful contribution to the inheritance of later segmentation methods. Second, by initializing the contour as a signed distance function (SDF), there are difficulties of keeping its main property $|\nabla\phi| = 1$. Due to the periodically complex re-initialization process, expensive computation is required, and undesirable side effects of moving the zero level set away from initial location of the contour occur [21]. Li et al. [22,23] introduced a distance regularized level set evolution (DRLSE) algorithm to represent a new variational formulation, which completely eliminated the need for a costly re-initialization procedure.

According to the nature of color images, it is worthwhile to inherit strong points of edge-based models, with different region-based information cues. In this paper, we explore good characteristics of both the Chan-Vese method, and the DRLSE approach. We use the geometric active contour model which provides flexible abilities for complex and changeable topology. Moreover, direct handling of color images helps us to avoid time-consuming gray-scale conversion steps, and the loss of color characteristics.

Major contributions of our work include the following.

- We can model effectively both edge information and adaptive region information to the energy functional of LSM.
- The need for a gray-scale conversion step can be removed.
- The boundary of the object of interest can be fitted accurately, despite the users' flexible initialization.
- We can balance the accuracy and computational time of the algorithm.

The paper is organized as follows. In Section 2, we describe our novel active contour model, and additional concepts. After that, Section 3 provides experimental results to illustrate the performance on a public database. Finally, we give detailed analysis and conclusions, as well as discuss our further works, in Section 4.

2. **A Novel Morphological Gradient-Based Active Contour Model.** In this paper, we concentrate on solving the problem of object segmentation for color images. Although there are a lot of researches, this process has still been a considerable task, because of difficulties related to not only the computational cost, but also the identification of object boundaries, due to both color characteristics, and contour initialization. Since promising results have been shown, DRLSE is adapted to the basic requirements of our model.

This approach was originally developed to suit gray-scale images. Normally most of edge-based segmentation methods convert color images to gray-scale, before detecting edge information. Consequently, the model spends much time on the conversion, as well as substantial edge information being lost (see Figure 1). To reduce these limitations, we calculate the gradient value directly in the original input (i.e., natural images), to take full advantage of color characteristics.

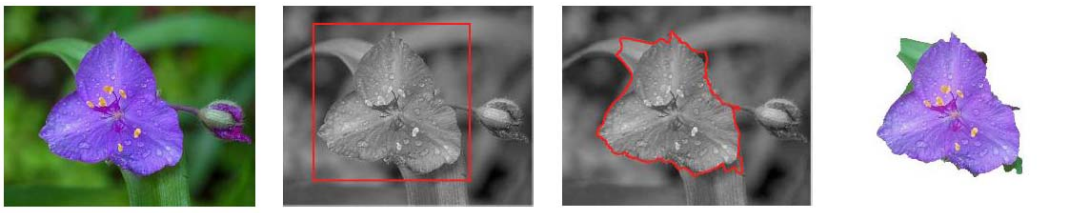

(a) Color image (b) Gray-scale conversion with a red initial contour (c) Incorrect result caused by lost real edge information (d) Segmented object

FIGURE 1. Color object segmentation by DRLSE in the case of using gray-scale conversion

In natural images, object boundaries may be weak to distinguish, because there are various colors that are nearly the same in the RGB space. Furthermore, colors of both objects and background may be non-homogeneous. Normal gradient-based edge detectors may not adequately exploit boundary characteristics, or control the effect of colors. In this paper, to increase the confidence of the supplied edge information, we calculate a precise edge map by using morphological gradient, combined with the squared local contrast (SLC) method.

2.1. **Morphological gradient-based edge detector.** To detect edges, the gradient value of an image is usually computed. Among current edge detectors, the morphological gradient is a simple and effective method that calculates the difference between maximum and minimum values over neighborhoods of pixels, by dilation and erosion operators. To build this edge map, morphological operators require scalar, or gray-scale, inputs only. In this case, color images are our obstacle. Cumani [25] proposed the squared local

contrast (SLC) method whose result has become a good input for morphological gradient computation and even enhances the value of real object boundaries.

We start by considering a color image as a two-dimensional vector field $I(x, y)$ with each element containing three values in proportion to the R, G and B channels. In this case, the squared local contrast $S(P; \vec{a})$ of a point $P(x, y)$ defines the squared norm of the directional derivative of I in the direction of the unit vector $\vec{a} = (a_1, a_2)$. This is expressed as below:

$$\begin{aligned} S(P; \vec{a}) &= \frac{\partial I}{\partial x} \cdot \frac{\partial I}{\partial x} \cdot a_1 \cdot a_1 + 2 \cdot \frac{\partial I}{\partial x} \cdot \frac{\partial I}{\partial y} \cdot a_1 \cdot a_2 + \frac{\partial I}{\partial y} \cdot \frac{\partial I}{\partial y} \cdot a_2 \cdot a_2 \\ &= E \cdot a_1^2 + 2 \cdot F \cdot a_1 \cdot a_2 + G \cdot a_2^2 \end{aligned} \tag{1}$$

Here

$$\begin{aligned} E &= \frac{\partial I}{\partial x} \cdot \frac{\partial I}{\partial x} = \sum_{i=1}^{3} \frac{\partial I_i}{\partial x} \cdot \frac{\partial I_i}{\partial x} \\ F &= \frac{\partial I}{\partial x} \cdot \frac{\partial I}{\partial y} = \sum_{i=1}^{3} \frac{\partial I_i}{\partial x} \cdot \frac{\partial I_i}{\partial y} \\ G &= \frac{\partial I}{\partial y} \cdot \frac{\partial I}{\partial y} = \sum_{i=1}^{3} \frac{\partial I_i}{\partial y} \cdot \frac{\partial I_i}{\partial y} \end{aligned} \tag{2}$$

The eigenvalues $\lambda_\pm$ of the following matrix $M = \begin{pmatrix} E & F \\ F & G \end{pmatrix}$, or metric tensor in the notation of Riemannian geometry [26], coincide with the extreme values of $S(P; \vec{a})$. These extreme values have the forms of

$$\lambda_\pm = \frac{E + G}{2} \pm \sqrt{\frac{(E - G)^2}{4} + F^2} \tag{3}$$

Values of λ_+ and λ_- describe the maximal and minimal rate of change in images, respectively. In gray-scale images, the "strength" of edges is the magnitude of the maximum gradient. However, in color images, as in [26], its "strength" should be the comparison between λ_+ and λ_-. So the edge map can be given as

$$f_{edge\_map} = f(\lambda_+, \lambda_-) = \lambda_+ - \lambda_- \tag{4}$$

We then calculate its gradient value $\nabla_B(f_{edge\_map})$ by applying the morphological gradient method as

$$\nabla_B(f_{edge\_map}) = \delta_B(f_{edge\_map}) - \varepsilon_B(f_{edge\_map}) \tag{5}$$

where δ and ε are the morphological dilation and erosion respectively, and B is a flat structuring element.

In the given result the value of each pixel indicates the strength of its contrast to its close neighborhood. It is important to emphasize that gradient peaks are located on edges. For this reason, we use the above morphological gradient map to compute a stopping term as

$$g_{color} = \frac{1}{1 + \nabla_B(f_{edge\_map})} \tag{6}$$

In traditional active contour methods (e.g., DRLSE), initial contours should be close enough to the boundary of desired objects. If contours are initialized that are intersecting or quite far from real boundaries, edge-based models cannot control their evolution to the correct edge pixels despite their gradient value being high. A common piecewise constant

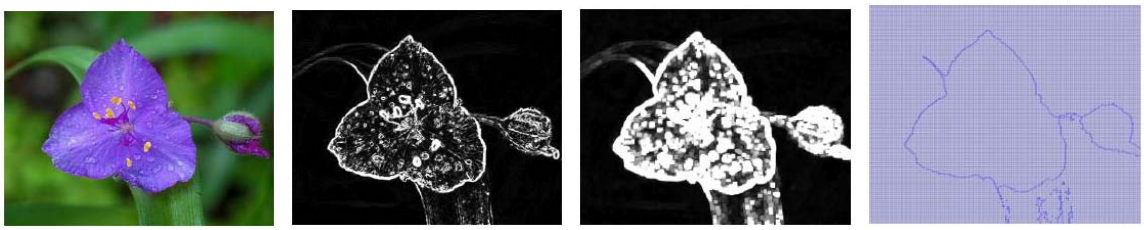

(a) Original image (b) f_{edge_map} (c) $\nabla_B(f_{edge\_map})$ (d) Gradient image

FIGURE 2. Morphological gradient-based method for edge detection

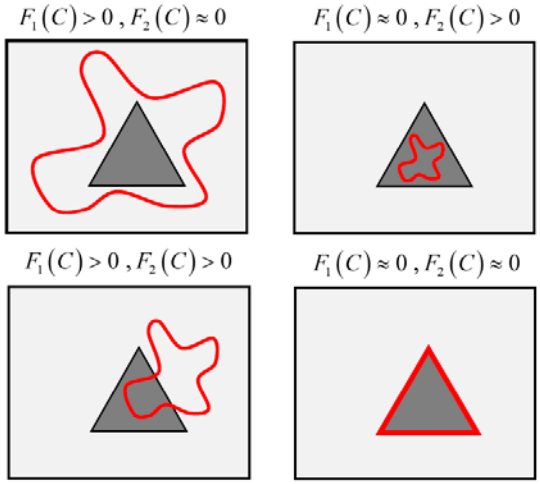

FIGURE 3. All possible cases of the Chan-Vese minimal variance criterion

minimal variance criterion based on the Mumford-Shah function [27] was proposed by Chan and Vese [17] to deal with this issue.

2.2. **A modified Chan-Vese minimal variance criterion.** The Chan-Vese model uses regional statistic information, and has the advantage of a regional model. When adding regional information into an energy function, the convergence space can expand and the initialization can be more flexible [20]. This idea is shown briefly in Figure 3.

The Chan-Vese minimal variance criterion, sometimes called the fitting term, is given by

$$F_1(C) + F_2(C) = \omega_1 \int_{inside\,C} (I_g - c_1)^2 dxdy + \omega_2 \int_{outside\,C} (I_g - c_2)^2 dxdy \tag{7}$$

where C is any variable curve, and the optimal c_1, c_2 depending on C are the averages of a gray-scale I_g inside and outside C, respectively. If C is exactly on the object boundary, then $F_1(C) \approx 0$, $F_2(C) \approx 0$, and the fitting term is minimized. ω_1, $\omega_2 > 0$ are weights which control the evolving speed of the curve.

Compared with the color input, the stopping term g_{color} can depict object boundaries more precisely and reliably in the range of [0, 255]. So, in this whole paper, we replace the gray-scale image I_g in Equation (7) with g_{color}, to improve performance of our model. By taking the derivative of Equation (7) with respect to the curve C, the first variation is

$$\frac{\partial F_1}{\partial C} + \frac{\partial F_2}{\partial C} = \left[-\omega_1 (g_{color} - c_1)^2 + \omega_2 (g_{color} - c_2)^2\right] \tag{8}$$

Here c_1, c_2 are the average intensities of g_{color} inside and outside the contour and are computed as

$$\begin{aligned} c_1(\phi) &= \frac{\int_\Omega g_{color} H(\phi) d\vec{x}}{\int_\Omega H(\phi) d\vec{x}} \\ c_2(\phi) &= \frac{\int_\Omega g_{color}(1 - H(\phi)) d\vec{x}}{\int_\Omega (1 - H(\phi)) d\vec{x}} \end{aligned} \tag{9}$$

where $H(\phi) = \begin{cases} 1 & \text{if } \phi \geq 0 \\ 0 & \text{if } \phi < 0 \end{cases}$ is a Heaviside step function. It is commonly difficult to correctly tune weight parameters in Equation (8). They are usually fixed by experiments for separate datasets. To let them adapt to each image, a measure of information content, which is image entropy is defined as

$$\begin{aligned} E_{in} &= -\sum_{k=1}^{n} p_k \log_2 p_k \quad (k \in inside(C)) \\ E_{out} &= -\sum_{k=1}^{n} p_k \log_2 p_k \quad (k \in outside(C)) \end{aligned} \tag{10}$$

where p_k is the probability of the k^{th} color level. These values reflect the diversity of the intensity of the image. To help the Chan-Vese criterion provide more adaptive region information, we assume that

$$\begin{aligned} \omega_1 &= E_{in} \\ \omega_2 &= E_{out} \end{aligned} \tag{11}$$

2.3. **A novel morphological gradient-based active contour model.** As mentioned before, DRLSE is chosen as the fundamental energy functional. In this paper, we try enhancing its two limitations, related to color images and flexible contour initialization.

In this approach, its energy functional was introduced as the following:

$$\varepsilon(\phi) = \mu R_p(\phi) + \varepsilon_{ext}(\phi) \tag{12}$$

where $R_p(\phi)$ is the level set regularization term to characterize how close the LSF ϕ is to an SDF, μ is a constant controlling this deviation, and $\varepsilon_{ext}(\phi)$ is a certain external term, depending on the desired image features.

The regularization term has the meaning of an internal energy term, which penalizes the deviation of ϕ from an SDF during its evolution. This term was defined as

$$R_p(\phi) = \int_\Omega p(\nabla\phi) d\vec{x} \tag{13}$$

where p is a potential function. In this paper, we choose a double-well potential function as follows:

$$p(s) = \begin{cases} \frac{1}{(2\pi)^2}(1 - \cos(2\pi s)) & \text{if } s \leq 1 \\ \frac{1}{2}(s-1)^2 & \text{if } s \geq 1 \end{cases} \tag{14}$$

The external energy term in Equation (12) derives the zero level set toward the object boundaries. Different from the original formula in [22,23] for helping DRLSE to detect real object boundaries accurately and quickly in color images, we use the edge map g_{color} defined in Equation (6) rather than its normal edge indicator g, as below

$$\varepsilon_{ext}(\phi) = \lambda \int_\Omega g_{color} \delta(\phi) |\nabla\phi| d\vec{x} + v \int_\Omega g_{color} H(-\phi) d\vec{x} \tag{15}$$

where $\lambda > 0$, and $v \in R$. Here, δ is the univariate Dirac function defined by $\delta(\phi) = H'(\phi)$. In the right-hand side term, the first component computes the length of the zero level

FIGURE 4. Segmentation in the case that the energy functional does not add regional information

contour of ϕ. This energy is minimized, when the zero level contour of ϕ is located at the object boundaries. The second component computes the weighted area of the region inside the contour ϕ, as well as allowing speeding up the motion of the zero level contour of ϕ.

In the case that the initial contours are inside, or enclose the object of interest completely, this approach seems good enough. The contour just needs to deform, by either shrinking or expanding, in only the one direction. However, for cases in which a contour is initialized arbitrarily, users may not know where the contour should move, to fix its deformable direction. Illustrations of these restrictions are shown in Figure 4. The original image with an arbitrary initial contour is represented in Figure 4(a). When the energy functional of DRLSE does not include regional information, segmentation results after 140 iterations are demonstrated in Figures 4(b) and 4(c). In the case of Figure 4(b), the closed curve will shrink, when the speed function propagates in the normal direction. Otherwise, the contour will expand and disappear in Figure 4(c). They show that the model cannot achieve our expected result, as in Figure 4(d).

To let DRLSE in Equation (15) control the deformation of the contour better and with more precision, regional information should be added to its energy functional as the second constraint. According to the Chan-Vese minimal variance criterion in Section 2.2, our novel segmentation algorithm is proposed, that integrates both types of information. Finally, for a level set function ϕ, we define a new energy functional $\varepsilon(\phi)$ as

$$\begin{aligned}\varepsilon(\phi) = \mu R_p(\phi) + \lambda \int_\Omega g_{color}\delta(\phi)|\nabla\phi|d\vec{x} + v\int_\Omega g_{color}H(-\phi)d\vec{x} \\ + \omega_1\int_\Omega (g_{color}-c_1)^2 d\vec{x} + \omega_2\int_\Omega (g_{color}-c_2)^2 d\vec{x}\end{aligned} \tag{16}$$

Lastly, to minimize the energy functional $\varepsilon(\phi)$ in Equation (16) the derivative of the LSF with respect to t is taken. Using the calculus of variations [16], the steepest descent process for the minimization of Equation (16) can be written as

$$\begin{aligned}\frac{\partial\phi}{\partial t} = \mu\left(\Delta\phi - div\left(\frac{\nabla\phi}{|\nabla\phi|}\right)\right) + \lambda\delta(\phi)div\left(g_{color}\frac{\nabla\phi}{|\nabla\phi|}\right) + vg_{color}\delta(\phi) \\ - \omega_1(g_{color}-c_1)^2 + \omega_2(g_{color}-c_2)^2\end{aligned} \tag{17}$$

where Δ is the Laplacian operator.

This new model can shorten computational time and give more accurate performance. We call it the morphological gradient-based active contour model for color image segmentation.

In practice, to discretize Equation (17) for numerical implementation, the univariate Dirac function and Heaviside function in the external energy term are approximated by

smoothing functions as

$$\delta_\varepsilon(x) = \begin{cases} \frac{1}{2\varepsilon}\left[1+\cos\left(\frac{\pi x}{\varepsilon}\right)\right] & |x| \le \varepsilon \\ 0 & |x| > \varepsilon \end{cases} \tag{18}$$

$$H_\varepsilon(x) = \begin{cases} \frac{1}{2}\left[1+\frac{x}{\varepsilon}+\frac{1}{\pi}\sin\left(\frac{\pi x}{\varepsilon}\right)\right] & |x| \le \varepsilon \\ 1 & x > \varepsilon \\ 0 & x < -\varepsilon \end{cases} \tag{19}$$

where ε is a constant chosen by experiments.

More flexibly, the initial contour ϕ_0 can be defined as an SDF or even a simple binary step function

$$\phi_0(x) = \begin{cases} -c_0 & \text{if } x \in R_0 \\ c_0 & \text{otherwise} \end{cases} \tag{20}$$

where R_0 is a particular region in the image domain, and $c_0 > 0$ is constant. Then the discretization of evolution Equation (17) is followed by the forward difference scheme, and expressed by the differential equation below

$$\phi_{i,j}^{k+1} = \phi_{i,j}^{k} + \tau L(\phi_{i,j}^{k}) \tag{21}$$

where $L(\phi_{i,j}^{k})$ is an approximation of the right hand side in Equation (17) using the spatial difference scheme, including central difference for partial derivatives, and forward difference for the temporal derivative.

3. **Experimental Results.** To demonstrate performance of our proposed algorithm for natural color images, we have carried out different evaluations on a public database provided by Achanta et al. [29]. This program runs on a PC equipped with Intel(R) Core$^{\text{TM}}$2 CPU 6700 @2.66GHz 2.67GHz and 2GB RAM in the environment of Matlab 2011a. For all experiments in this paper, we fixed the value of parameters as $\mu = 0.02$, $\lambda = 5$, $v = 3$, $\varepsilon = 1.5$ and the time step $\tau = 10$.

Average precision, recall, and F-measure are used to measure the performance of results over their ground truth among them, and F-measure is defined as

$$F\text{-measure} = \frac{(1+\beta^2)(\text{Precision} \times \text{Recall})}{\beta^2 \text{Precision} + \text{Recall}} \tag{22}$$

The relative weight between the precision and recall controlled by β^2 is set to 0.5 to give an equal weight to these metrics.

3.1. **Experiment 1: Flexible contour initialization.** In this case, an illustration of the effectiveness of our proposed ACM is studied by using regional information.

There are three common positions to locate initial contours relative to objects of interest in images. As shown in Figures 6(a)-6(c), the contours are sequentially initialized completely outside, completely inside, or partly intersecting the desired object respectively. Despite their placements in the image, applying our novel ACM can control their

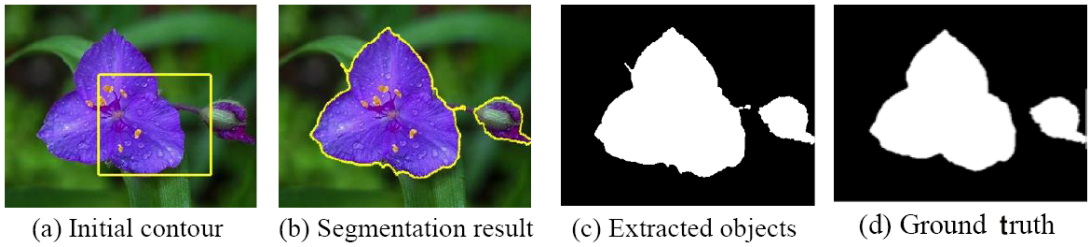

(a) Initial contour (b) Segmentation result (c) Extracted objects (d) Ground truth

FIGURE 5. Flower segmentation result by our proposed method

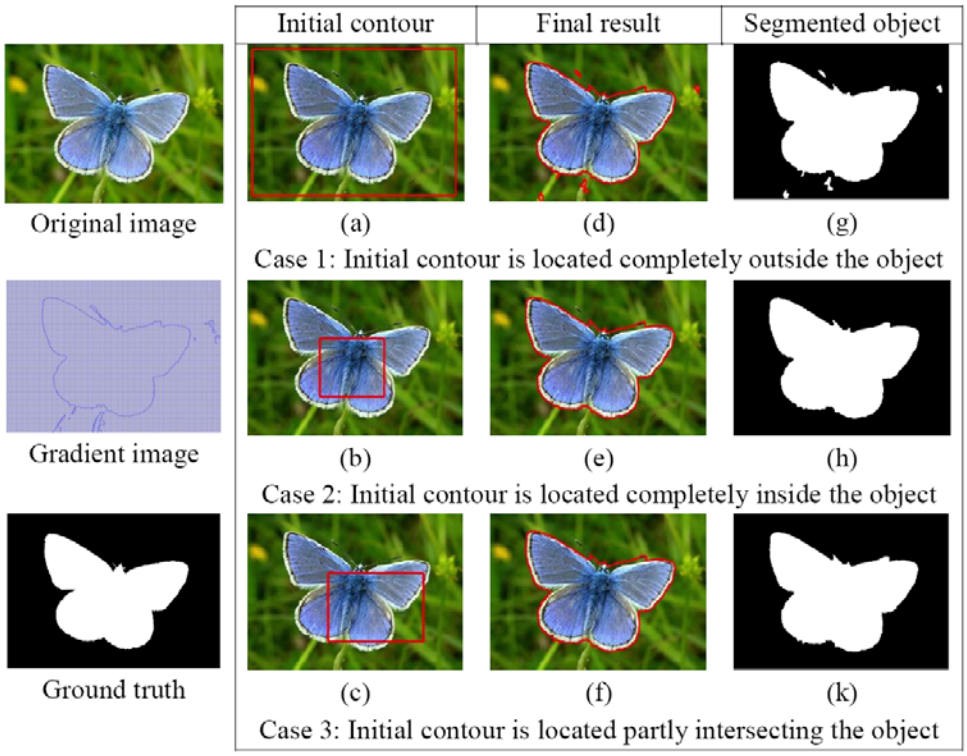

FIGURE 6. Segmentation results of different initial locations of the active contour

evolution towards the exact object boundary. From comparing segmented objects in the third column to its ground truth, they are almost similar in all of the cases.

Additionally, this case study is helpful in depicting the relationship of the running time to the size and position of initial curves. The original input is a 400×290 image captured in RGB color space. When the contour starts from bounding the whole object (i.e., case 1), our program will take both a lesser number of iterations and a shorter period time than the other two cases (i.e., cases 2 and 3). In detail, the final result in Figure 6(g) was caught after 85 iterations in only 34 seconds. Conversely, to achieve Figures 6(h) and 6(k), the contour stopped after 200 steps of evolution in more than 80 seconds.

3.2. **Experiment 2: Efficient edge map computation.** In this case, a practical example is studied to illustrate our good performance achieved by a new combination of two simple methods for edge detection.

First, we show a step-by-step experiment of the segmentation performed by our novel ACM to a 400×265 color image (see Figure 7(a)). The initial contour is represented as a yellow rectangle in Figure 7(b). At first, the SLC method is used to keep good characteristics in the input while reducing its number of color channels (see Figure 7(c)). After that, we apply the morphological gradient method to compute its edge map, as shown in Figure 7(d). Next, Figures 7(e)-7(g) are evolution of the contour of the order of 60^{th}, 120^{th} and 180^{th} iterations at 5.1, 10.1 and 15.2 seconds, respectively. Finally, Figure 7(h) demonstrates that the obtained object is accurate and looks quite smooth at its boundary.

As mentioned before, this improvement in our proposed ACM can help avoid the following weaknesses:

- Waste of time and loss of edge characteristics caused by gray-scale conversion
- Weak distinction of boundary between object and background
- Non-homogeneity coloring inside objects and background

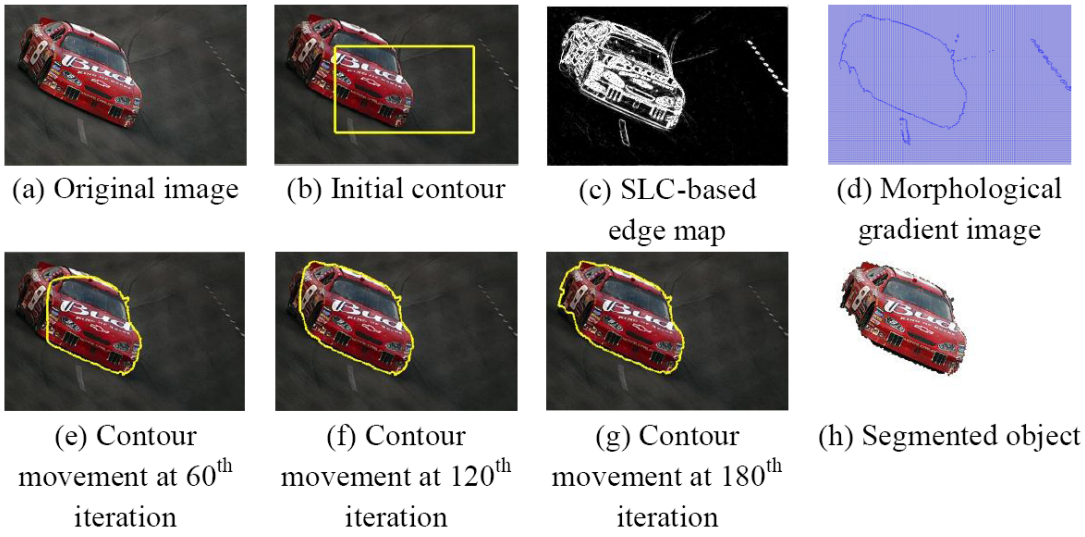

(a) Original image (b) Initial contour (c) SLC-based edge map (d) Morphological gradient image

(e) Contour movement at 60th iteration (f) Contour movement at 120th iteration (g) Contour movement at 180th iteration (h) Segmented object

FIGURE 7. Segmentation results performed by our morphological gradient-based ACM

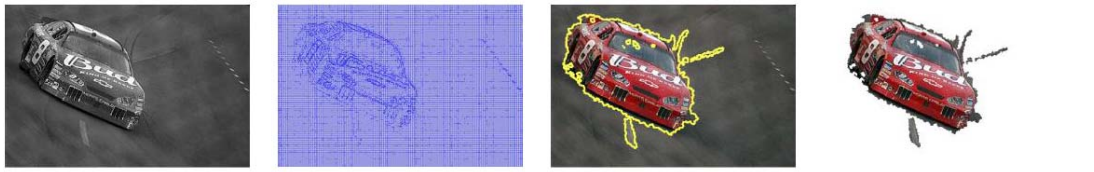

(a) Gray-scale conversion (b) Gradient image (c) Contour stops at 350th iteration (d) Segmented object

FIGURE 8. Segmentation results performed by a normal gradient-based ACM with gray-scale conversion

To further clarify the significance of our novel technique, we visually compare the performance between our model and normal segmentation approaches. Figure 8 describes the corresponding process of segmentation based on normal gradient-based edge detection. The original input in Figure 7(a) is first converted to gray-scale as in Figure 8(a). In Figure 8(b), the derivatives of the gray-scale image with respect to x- and y-coordinates are then taken to compute the gradient value. To achieve a fair comparison, our g_{color} in Equation (17) is replaced by the gradient image in Figure 8(b) to control movement of the initial contour. To attain the segmented object in Figure 8(d), it finally takes over 350 steps of evolution for 53.8 seconds. By comparison, it is easy to observe that the contour in Figure 8(c) is more coarse and does not bound the car more precisely than ours in Figure 7(g).

3.3. **Experiment 3: Comparison between the current work and existing ones.** In this case, we compare the performance of our morphological gradient-based ACM with four other segmentation methods for both accuracy and computational time. The chosen approaches are

- The RGAC model [30]
- The vector-valued Chan-Vese model [31]
- The Fixation-based active model [32]
- The Marker-based watershed [33]

By applying these methods to the entire public Achanta database, the performance is summarized in Table 1. Overall our model provides a much superior balance of accuracy and computational time. Compared with the two chosen deformable models [30,31], our model shows much better effectiveness as well as faster manipulation. Although two other segmentation models [32,33] spend much less processing time than our model, their segmenting performance heavily depends on user-specified seed locations. With the fixation-based active model, different initial points inside the object of interest will give

FIGURE 9. Visual segmentation comparison between our proposed method and various segmentation models

TABLE 1. Performance of various segmentation methods on the public database [29]

Method	**Precision**	**Recall**	***F*-measure**	**Average processing time (seconds)**	**Programming language**
Our proposed method	0.79	0.81	0.80	15.7	Matlab
RGAC	0.50	0.77	0.57	25.1	Matlab
C-V model for vector-valued image	0.58	0.58	0.58	35.8	Matlab
Fixation-based active model	0.80	0.72		2.1	C
Marker-based watershed	0.66	0.84	0.71	0.15	C

different results. So it cannot perform really stable segmentation. With the marker-based watershed method, its performance depends on how users draw the background and foreground markers. If a foreground marker includes a small part of the background, it will produce a wrong result, and vice versa.

To clarify the comparison more clearly, a visual example is given in Figure 9. With each model, user interactions generate initial seeds, as shown in Figures 9(c)-9(k) respectively. Then, segmenting results are reached in turn, corresponding to their initialization in Figures 9(h)-9(r). In this figure, we also show two results of the fixation-based active model and marker-based watershed achieved by two different initializations. Compared with all chosen methods, our result finally obtains a smoother, more exact contour (84% of accuracy) and in less computing time (during 14 seconds) in Figure 9(l).

4. **Conclusions.** In this paper, we presented a novel active contour model to solve this problem without the need of a gray-scale conversion step or hard initial contours. By combining the morphological gradient of a squared local contrast image and the DRLSE method both edge information and regional information is used to propagate an initial curve that finds the desired object boundaries smoothly and exactly. The experiments have shown that it achieves more convincing and encouraging results than the other deformable models in terms of effectiveness and efficiency. Even though these are worthwhile improvements, our algorithm still has some limitations. In the future, we will investigate:

- Decreasing the adverse effect of the size of initial contours on processing time;
- Extracting more effective information from color images (e.g., texture) to achieve more precise results.

Acknowledgement. This research was supported by Basic Science Research Program through NRF funded by the Ministry of Education, Science and Technologies (2012-047759) and the MSIP (Ministry of Science, ICT & Future Planning), Korea, under the ITRC (Information Technology Research Center) support program supervised by the NIPA (National IT Industry Promotion Agency) (NIPA-2013-H0301-13-3005).

REFERENCES

[1] M. Fussenegger, A. Opelt, A. Pinz and P. Auer, Object recognition using segmentation for feature detection, *Proc. of IEEE Int. Conf. Pattern Recognition*, pp.41-44, 2004.

[2] K. Hirata, E. Kasutani and Y. Hara, On image segmentation for object-based image retrieval, *Proc. of IEEE Int. Conf. Pattern Recognition*, pp.1031-1034, 2002.

[3] W. A. Barrett and A. S. Cheney, Object-based image editing, *ACM Trans. on Graph.*, vol.21, no.3, pp.777-784, 2002.

[4] A. K. Agrawal and R. Chellappa, Moving object segmentation and dynamic scene reconstruction using two frames, *Acoustics, Speech, and Signal Processing*, vol.2, pp.705-708, 2005.
[5] R. Achanta, Frequency-tuned salient region detection, *Computer Vision and Pattern Recognition*, pp.1597-1604, 2009.
[6] M.-M. Cheng, Global contrast based salient region detection, *Computer Vision and Pattern Recognition*, pp.409-416, 2011.
[7] Y. Y. Chuang, B. Curless, D. H. Salesin and R. Szeliski, A Bayesian approach to digital matting, *Proc. of IEEE International Conference on Computer Vision and Pattern Recognition*, pp.264-271, 2001.
[8] F. Meyer, Topographic distance and watershed lines, *Signal Processing*, vol.38, pp.113-125, 1994.
[9] Y. Boykov and G. Funka-Lea, Graph cuts and efficient N-D image segmentation, *Int. J. Computer Vision*, vol.70, no.2, pp.109-131, 2006.
[10] C. Rother, V. Kolmogorov and A. Blake, GrabCut – Interactive foreground extraction using iterated graph cuts, *Proc. of ACM SIGGRAPH*, pp.309-314, 2004.
[11] M. Kass, A. Witkin and D. Terzopoulous, Snakes: Active contour models, *International Journal of Computer Vision*, vol.1, pp.321-331, 1987.
[12] S. Osher and J. Sethian, Fronts propagating with curvature-dependent speed: Algorithms based on Hamilton-Jacobi formulations, *Journal of Computational Physics*, vol.79, pp.12-49, 1988.
[13] V. Caselles, R. Kimmel and G. Sapiro, Geodesic active contours, *International Journal of Computer Vision*, vol.22, no.1, pp.61-79, 1997.
[14] C. Xu and J. L. Prince, Gradient vector flow: A new external force for snakes, *IEEE Proc. of Conference on Computer Vision and Pattern Recognition*, pp.66-71, 1997.
[15] S. Osher and R. Fedkiw, *Level Set Methods and Dynamic Implicit Surfaces*, Springer, New York, 2003.
[16] J. A. Sethian, *Level Set Methods and Fast Marching Methods*, Cambridge University Press, Cambridge, 1999.
[17] T. F. Chan and L. A. Vese, Active contours without edges, *IEEE Trans. on Image Processing*, vol.10, no.2, pp.266-277, 2001.
[18] W. Chen, Gradient vector flow using an implicit method, *International Journal of Information Technology*, vol.12, no.2, pp.14-23, 2006.
[19] C. Li, C. Y. Kao, J. C. Gore and Z. H. Ding, Minimization of region-scalable fitting energy for image segmentation, *IEEE Trans. on Images Processing*, vol.17, no.10, 2008.
[20] D. Cremers, M. Rousson and R. Deriche, A review of statistical approaches to level set segmentation: Integrating colors, texture, motion and shape, *International Journal of Computer Vision*, vol.72, pp.192-215, 2007.
[21] Y. Zheng, G. Li, X. Sun and X. Zhou, A geometric active contour model without re-initialization for color images, *Image and Vision Computing*, vol.27, pp.1411-1417, 2009.
[22] C. Li, C. Xu, C. Gui and M. D. Fox, Level set evolution without re-initialization: A new variational formulation, *Proc. of the 2005 IEEE Computer Society Conference on Computer Vision and Pattern Recognition*, vol.1, pp.430-436, 2005.
[23] C. Li, C. Xu, C. Gui and M. D. Fox, Distance regularized level set evolution and its application to image segmentation, *IEEE Trans. on Image Processing*, vol.19, no.12, pp.3243-3254, 2010.
[24] L. Chen, Y. Zhou, Y. Wang and J. Yang, GACV: Geodesic-aided C-V method, *Journal of the Pattern Recognition Society*, vol.39, pp.1391-1395, 2006.
[25] A. Cumani, Edge detection in multi-spectral images, *CVGIP: Graphical Models and Image Processing*, vol.53, no.1, pp.40-51, 1991.
[26] G. Sapiro, Color snakes, *Computer Vision and Image Understanding*, vol.68, pp.247-253, 1997.
[27] D. Mumford and J. Shah, Optimal approximation by piecewise smooths functions and associated variational problems, *Communications on Pure and Applied Mathematics*, vol.42, pp.577-685, 1989.
[28] B. V. Dhandra and R. Hegadi, Active contours without edges and curvature analysis for endoscopic image classification, *International Journal of Computer Science and Security*, vol.1, no.1, pp.19-32, 2007.
[29] *http://ivrgwww.epfl.ch/supplementary_material/RK_CVPR09/index.html.*
[30] H. J. Wang, M. Liu and W. L. Ma, Color image segmentation based on a new geometric active contour model, *IEEE International Conference on Machine Vision and Human-Machine Interface*, pp.6-9, 2010.
[31] T. F. Chan, B. Y. Sandberg and L. A. Vese, Active contours without edges for vector-valued images, *Journal of Visual Communication and Image Representation*, pp.130-141, 2000.

[32] A. K. Mishra, Y. Aloimonos, L. F. Cheong and A. A. Kassim, Active visual segmentation, *IEEE Trans. on Pattern Analysis and Machine Intelligence*, vol.34, no.4, pp.639-653, 2012.

[33] F. Meyer, Un algorithme optimal de partage des eaux, *Proc. of the 8th Congress AFCET*, Lyon-Villeurbanne, France, vol.2, pp.847-859, 1991.